Quantitative analysis of precise heavy-ion fusion data at above-barrier energies using Skyrme-Hartree-Fock nuclear densities

I. I. Gontchar,[1] R. Bhattacharya,[2] and M. V. Chushnyakova[1,*]
[1]*Physics Department, Omsk State Technical University, Omsk, Russia*
[2]*Department of Physics, University of Calcutta, Kolkata, India*
(Received 29 October 2013; revised manuscript received 4 January 2014; published 3 March 2014)

We calculate the capture (fusion) cross sections for nine reactions involving spherical nuclei: $^{16}O + ^{16}O$, ^{28}Si, ^{92}Zr, ^{144}Sm, ^{208}Pb; $^{28}Si + ^{28}Si$, ^{92}Zr, ^{208}Pb; $^{32}S + ^{208}Pb$. For six of them precision data are available in the literature. Analysis of these precision data within the framework of the single-barrier penetration model based on the Woods-Saxon profile for the strong nucleus-nucleus interaction potential (SnnP) gave rise to the problem of the apparently large diffuseness of the SnnP [Newton *et al.*, Phys. Rev. C **70**, 024605 (2004)]. Our fluctuation-dissipation trajectory model is based on the double-folding approach with the density-dependent M3Y *NN* forces including the finite-range exchange part. For the nuclear matter density the Skyrme-Hartree-Fock approach including the tensor interaction is applied. The resulting nucleus-nucleus potential possesses rather small (normal) diffuseness. The strength of the radial friction K_R is used as the free parameter of the model. It turns out that for four of the five reactions induced by ^{16}O (except $^{16}O + ^{208}Pb$) the calculated cross sections cannot be brought into agreement with the data within the experimental errors. This suggests that the calculated nuclear density is incorrect for ^{16}O. For the reactions not involving ^{16}O and, surprisingly, for the $^{16}O + ^{208}Pb$ reaction the agreement with the data within 2-5% is achieved at $K_R = 1.2 \times 10^{-2}$ to 3.0×10^{-2} MeV^{-1} zs which is in accord with the previous works.

DOI: 10.1103/PhysRevC.89.034601 PACS number(s): 25.70.Jj, 25.60.Pj, 24.10.−i

I. INTRODUCTION

The experimental data on the capture cross sections σ in heavy-ion collisions have so far been systematically analyzed mostly within the framework of the coupled-channels approach [1–3]. The nucleus-nucleus strong interaction potential (SnnP) is the crucial ingredient of this approach. Conventionally, the Woods-Saxon (WS) profile

$$U_n(R) = V_{\rm WS}\left\{1 + \exp\left(\frac{R - r_{\rm WS}\left(A_P^{1/3} + A_T^{1/3}\right)}{a_{\rm WS}}\right)\right\}^{-1} \tag{1}$$

is used for the SnnP. In Eq. (1) R denotes the distance between the centers of mass of two spherical nuclei: the projectile with the mass number A_P and the target of the mass number A_T. The WS profile is defined by three parameters: the depth $V_{\rm WS}$, the radius parameter $r_{\rm WS}$, and the diffuseness $a_{\rm WS}$.

It was recognized [3] that at collision energies well above the Coulomb barrier the couplings to the excited states of the colliding nuclei do not influence the value of the cross section within 1%. Therefore the systematic analysis of the experimental capture excitation functions for $\sigma > 200$ mb was performed in Ref. [3] within the framework of the single-barrier penetration model (BPM). This analysis led to the values of $a_{\rm WS}$ ranging between 0.75 and 1.5 fm with a trend for $a_{\rm WS}$ to increase as the system becomes heavier. This is significantly larger than the value of 0.65 fm, which is required by the elastic scattering data. It was pointed out in Ref. [3] that the abnormally large diffuseness might be an artifact masking some dynamical effects.

Following this idea, we undertook several efforts [4–6] to analyze the experimental capture excitation functions using the dynamical model based on Langevin-type dissipative trajectories with the surface friction [7,8]. As in the case of the BPM, the SnnP is again a key part of the approach. In Refs. [7,8] the SnnP was calculated by means of folding the nucleus-nucleon optical potential with the nucleon density (single folding). Presently, a more microscopic double-folding (DF) SnnP with the density-dependent M3Y *NN* (nucleon-nucleon) forces [9,10] is available. Moreover, the data analyzed in Refs. [7,8] typically had an accuracy worse than 10%. In Ref. [3] the high-precision data (typically 1%) have been analyzed. Thus, it is tempting to apply the model based on the semimicroscopic DF potential for the analysis of these precision data in order to see whether accounting for the dynamical effects allows reproducing quantitatively the precision excitation functions without abnormally large diffuseness of the SnnP. Let us note that in Ref. [4] it was qualitatively shown that accounting for dissipation seems to be the right way to resolve this problem.

In the folding approach to the SnnP the nucleon (matter) density distributions are of great importance. For these densities usually the two-parameter Fermi ansatz is used:

$$\rho_A(r) = \rho_0\left\{1 + \exp\left(\frac{r - R_A}{a_A}\right)\right\}^{-1}. \tag{2}$$

Here ρ_0 is the parameter extracted from the normalization condition, and the diffuseness parameter a_A defines a surface layer thickness. Parameters R_A and a_A can be associated with those extracted from the experiments on the electron scattering [11], but in many cases they are unknown. In this paper we obtain the matter density distribution applying the microscopic Skyrme-Hartree-Fock (SHF) approach with

*Corresponding author: maira.chushnyakova@gmail.com

tensor forces. Thus the distribution is calculated without any assumptions about its shape.

There are two more differences between the present paper and Ref. [4]. First, the thermal fluctuations, ignored in Ref. [4], are accounted for in the present work. Second, whereas in Ref. [4] only qualitative comparison with the data was done, in the present paper we perform a quantitative comparison. This is of importance keeping in mind the small errors in the data analyzed. We are not aware of any publications devoted to the capture problem in which the results of a dynamical model are compared quantitatively with the data.

The paper is organized as follows. In Sec. II the data selected for the analysis are presented. The dynamical model as well as the SHF nuclear matter density is described in Sec. III. In Sec. IV the calculated cross sections are compared with the data and adjustment of the friction strength coefficient is done. In Sec. V conclusions are formulated.

II. SELECTING THE DATA FOR THE ANALYSIS

The capture cross section in the two spherical nuclei collision seems to be the simplest case for the analysis. We found the data corresponding to $\sigma > 200$ mb with the relative error about 1% on the following reactions [12]: $^{16}\mathrm{O}+{}^{92}\mathrm{Zr}$ [13], $^{16}\mathrm{O}+{}^{144}\mathrm{Sm}$ [14], $^{16}\mathrm{O}+{}^{208}\mathrm{Pb}$ [15], $^{28}\mathrm{Si}+{}^{92}\mathrm{Zr}$ [13], $^{28}\mathrm{Si}+{}^{208}\mathrm{Pb}$ [16], and $^{32}\mathrm{S}+{}^{208}\mathrm{Pb}$ [16]. Within the framework of these reactions we need to calculate the density distribution for the six nuclei: ^{16}O, ^{28}Si, ^{32}S, ^{92}Zr, ^{144}Sm, and ^{208}Pb. For other possible reactions involving these nuclei the data either are not found or possess the errors of about 10%. Since in the region $\sigma > 200$ mb the quantum fluctuations of the transmission coefficient are of minor importance, the data are expected to follow the simple trend

$$\sigma = \pi R_{B0}^2 \left(1 - \frac{U_{B0}}{E_{\mathrm{c.m.}}}\right), \tag{3}$$

which is the limiting case $U_{B0} < E_{\mathrm{c.m.}}$ of the Wong formula [17]. Here R_{B0} is the s-wave barrier radius, U_{B0} is the s-wave barrier height, $E_{\mathrm{c.m.}}$ is the collision energy in the center-of-mass frame. In Table I of Ref. [3] the values of R_{B0} and U_{B0} extracted from the data are presented. This enables us to check whether the data follow the trend (3) indeed. Result of such comparison is shown in Fig. 1. Reasonable universal linear behavior is seen. The thin dashed line corresponds to Eq. (3) times 0.9 whereas the thick solid line represents Eq. (3). Whatever the calculation is, the calculated cross sections must demonstrate the linear trend as the experimental data do. In Ref. [3] the energy-dependent barrier radius $R_E = R_{B0} - a_{\mathrm{WS}} \ln[1 + 2(E_{\mathrm{c.m.}} - U_{B0})/U_{B0}]$ was used. We cannot use this ansatz in our analysis (see Fig. 9 below) because we do not employ the Woods-Saxon profile for the SnnP.

III. MODEL

In our model, the fictitious particle with the reduced mass moves under the action of the conservative, dissipative, and stochastic forces. We consider the collision process at the energies well above the Coulomb barrier. So there is no need to account for quantum effects such as tunneling and channels coupling.

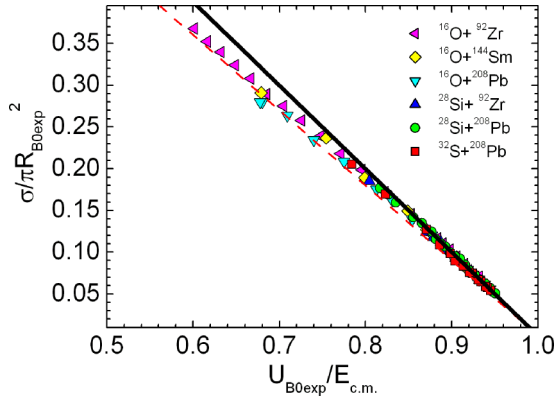

FIG. 1. (Color online) Reduced experimental cross sections vs $U_{B0\mathrm{expt}}/E_{\mathrm{c.m.}}$. Both $R_{B0\mathrm{expt}}$ and $U_{B0\mathrm{expt}}$ are taken from Ref. [3]. Thin dashed line corresponds to Eq. (3) times 0.9; the thick solid line represents Eq. (3). The data for the different reactions are taken from the following references: $^{16}\mathrm{O}+{}^{92}\mathrm{Zr}$ [13], $^{16}\mathrm{O}+{}^{144}\mathrm{Sm}$ [14], $^{16}\mathrm{O}+{}^{208}\mathrm{Pb}$ [15], $^{28}\mathrm{Si}+{}^{92}\mathrm{Zr}$ [13], $^{28}\mathrm{Si}+{}^{208}\mathrm{Pb}$ [16], and $^{32}\mathrm{S}+{}^{208}\mathrm{Pb}$ [16].

The spherical nuclei whose collision is considered in this work have usually at least one (proton or neutron) closed shell and are rather stiff. That is why we account for only one degree of freedom corresponding to the radial motion which is described by the dimensionless coordinate $q = R/R_{PT}$. Here R is the distance between the centers of the colliding nuclei, and R_{PT} is the sum of the half density radii of the projectile (P) and target (T) nucleus. The latter, being an important characteristic of the two-parameter Fermi (2pF) distribution, does not exist for the SHF distribution. Yet it is very convenient using the dimensionless dynamical coordinate q. Thus we put $R_{PT} = r_{\mathrm{GK}}(A_P^{1/3} + A_T^{1/3})$ where r_{GK} is defined below in Eqs. (11).

In our previous study [18] we accounted for the radial and orbital degrees of freedom solving four dynamical equations. We discussed there that ignoring two equations corresponding to the orbital motion influences the resulting cross sections within the framework of the statistical errors, which were typically 1%. Therefore in the present work we model dynamically only the radial motion, accounting, of course, for the angular-momentum dependence of the collision barrier.

Presently more sophisticated time-dependent Hartree-Fock (TDHF) [19–24] and quantum molecular dynamics [25] calculations of the heavy-ion collisions are available. In these works it was shown that the nucleon transfers [19] as well as the dynamical reagents deformation and neck formation [21,22] might be of importance. Although the probability of the nucleon transfer is known to increase with the collision energy, its effect on fusion is less important above the barrier [19]. In our calculations [4] for the reactions $^{16}\mathrm{O}+{}^{92}\mathrm{Zr}$, $^{16}\mathrm{O}+{}^{144}\mathrm{Sm}$, and $^{16}\mathrm{O}+{}^{208}\mathrm{Pb}$, capture was decided when $q > 1.25$ and the density in the overlap region was less than 25% of its central value (see, e.g., Fig. 9 of Ref. [26]). Thus, for the reactions considered in the present work, the neck certainly appears and the reagents deform but after the capture is decided (according to our criteria) and therefore beyond the framework of our model.

A. Dynamical equations

Our previous study demonstrated that the radial motion is rather fast. Namely, the calculations performed in Refs. [4,18] showed that the radial momentum was damped typically during 0.5-1.0 zs, whereas during this time lapse the orbital angular momentum lost at most several percent if its evolution was described by the classical dissipative equation [see, e.g., Eq. (11a) of Ref. [18]]. Therefore one could think that the stochastic equation for the radial degree of freedom has a non-Markovian shape. However, in the recent study [25] it was shown that retarding and non-Markovian effects appear near the contact point, i.e., when the center-of-mass distance is equal to the sum of the half density radii. Since in our model the contact point is never reached, we prefer to use the stochastic equation with the Gaussian noise and instant friction:

$$\frac{dp}{dt} = F_U + F_{\rm cen} + F_{Dq} + b\sqrt{2D_q}, \tag{4a}$$

$$\frac{dq}{dt} = \frac{p}{m_q}, \tag{4b}$$

$$F_U = -\frac{dU_{\rm tot}}{dq}, \tag{5a}$$

$$F_{\rm cen} = \frac{\hbar^2 L^2}{m_q q^3}, \tag{5b}$$

$$F_{Dq}(t) = -\frac{p(t)}{m_q} K_R \left(\frac{dU_n[q(t)]}{dq}\right)^2, \tag{6a}$$

$$D_q = \theta K_R \left(\frac{dU_n}{dq}\right)^2. \tag{6b}$$

Here p stands for the linear momentum corresponding to the radial motion ($[p] = \text{MeV} \cdot \text{zs}$); F_U, $F_{\rm cen}$, and F_{Dq} are the conservative, centrifugal, and dissipative forces, respectively ($[F_i] = \text{MeV}$). For the latter the surface friction expression [7,8] is used. $U_{\rm tot}(q)$ is the total interaction energy of two nuclei which consists of the Coulomb $U_C(q)$ and SnnP $U_n(q)$ parts ($[U] = \text{MeV}$); $\hbar L$ is the projection of the orbital angular momentum onto the axis perpendicular to the reaction plane ($[\hbar] = \text{MeV zs}$); $m_q = m_n A_P A_T \cdot R_{PT}^2 (A_P + A_T)^{-1}$ is the inertia parameter ($[m_q] = \text{MeV zs}^2$); m_n is the bare nucleon mass; K_R denotes the dissipation strength coefficient ($[K_R] = \text{MeV}^{-1}\,\text{zs}$). The diffusion coefficient D_q ($[D_q] = \text{MeV}^2\,\text{zs}$) is related to the temperature θ and friction coefficient $K_R \cdot (U_n')^2$ by the Einstein relation (6b).

The temperature θ is supposed to be the same for both collision partners. This assumption, although difficult to justify, is conventional for the dissipative dynamical models [27–31]. The temperature θ is calculated as follows:

$$\theta = \sqrt{E_{DP(T)} \left(a_1 A_{P(T)} + a_2 A_{P(T)}^{2/3}\right)^{-1}}, \tag{7}$$

where $a_1 = 0.073\ \text{MeV}^{-1}$ and $a_2 = 0.095\ \text{MeV}^{-1}$ [32]. The dissipated energy E_D is calculated according to the energy balance

$$E_D = E_{DP} + E_{DT} = E_{\rm c.m.} - \frac{p^2}{2m_q} - \frac{\hbar^2 L^2}{2m_q q^2} - U_{\rm tot}. \tag{8}$$

Equations (4) are solved applying the Runge-Kutta method (see Appendix B of [18]).

B. Capture cross sections

These cross sections are calculated according to the commonly used quantum-mechanical formula (see, e.g., [33])

$$\sigma = \frac{\pi \hbar^2}{2m_R E_{\rm c.m.}} \sum_{L=0}^{L_{\max}} (2L+1)\, T_L. \tag{9}$$

Here $m_R = m_n A_P A_T/(A_P + A_T)$, and $L_{\max}$ is the maximal angular momentum above which the transmission coefficient becomes equal to zero. In our work the transmission coefficient T_L is evaluated using either the dynamical approach or the single-barrier penetration model (BPM).

In the dynamical approach, typically $20 \cdot (2L+1)$ trajectories are simulated for every partial wave until the number of captured trajectories for the particular L becomes zero. The transmission coefficient is defined as the ratio of the captured trajectories number to the full number of trajectories for particular L value. The capture conditions were as described in Sec. II F of Ref. [4]. Namely, we assume the capture happens in one of the following two cases. First, two conditions must be fulfilled: (i) the radial coordinate of the particle must become smaller than the particular share (0.98) of the L-dependent barrier radius q_{BL}; and (ii) the radial kinetic energy must become smaller than the time-dependent temperature. The second case is when the trajectory penetrates beyond the barrier significantly deeper than in the first case: $q(t) < 0.5(1 + q_{BL})$.

Within the framework of the BPM using the parabolic barrier approximation the transmission coefficient reads [34]

$$T_L = \{1 + \exp[2\pi(U_{BL} - E_{\rm c.m.})/(\hbar\omega_{BL})]\}^{-1}. \tag{10}$$

Here U_{BL} and ω_{BL} are the barrier height and the barrier frequency for the particular L value. Typical transmission coefficients calculated using the BPM (lines without symbols) and the dynamical modeling (lines with symbols) are shown in Fig. 2 for the six reactions under consideration. For each reaction the BPM and dynamical modeling is done with the same potential. The collision energy in these calculations is about 10% larger than the s-wave barrier. One clearly sees the impact of friction and thermal fluctuations. Namely, for the reactions $^{16}\text{O} + ^{92}\text{Zr}$ and $^{16}\text{O} + ^{144}\text{Sm}$ both versions of the calculations result in rather close transmission coefficients. The only difference is that the dynamical transmission coefficient decreases steeper than the BPM T_L does because fusion at higher angular momenta is suppressed due to friction. In the case of the reactions $^{16}\text{O} + ^{208}\text{Pb}$ and $^{28}\text{Si} + ^{92}\text{Zr}$ the dynamical transmission coefficients (lines with symbols) are somewhat shifted left due to dissipation in comparison with the BPM. For the two heaviest reactions this shift and smearing due to thermal fluctuations appear in the strongest way. This trend is explained as follows. For the heavier system the barrier appears for the smaller values of q where the derivative of the SnnP is larger. This is seen in Table I. The longer is the path with the significant SnnP passed by the fictitious particle, the stronger is the resulting effect of the friction and fluctuations.

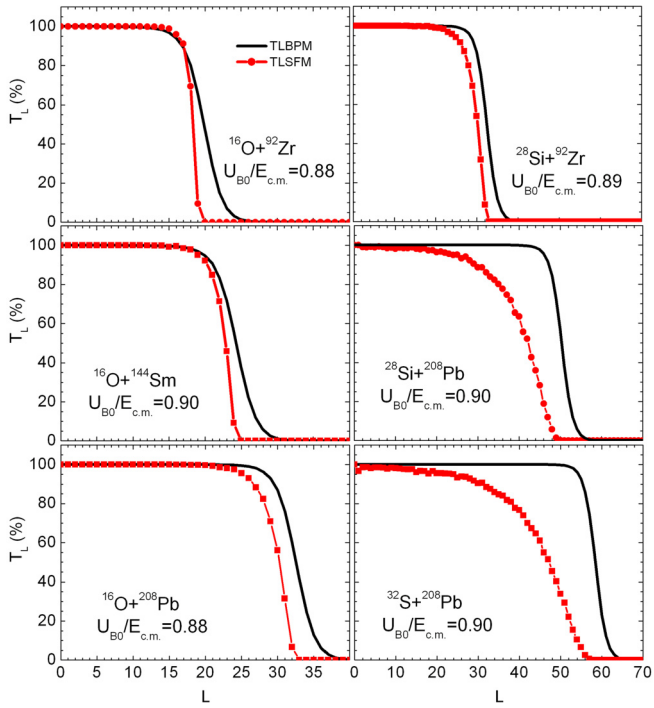

FIG. 2. (Color online) Transmission coefficients T_L calculated using the dynamical model (lines with symbols) and the BPM (lines without symbols). The values of $U_{B0}/E_{\text{c.m.}}$ corresponding to these calculations are indicated in the panels. $K_R = 2.0 \times 10^{-2}$ MeV^{-1} zs.

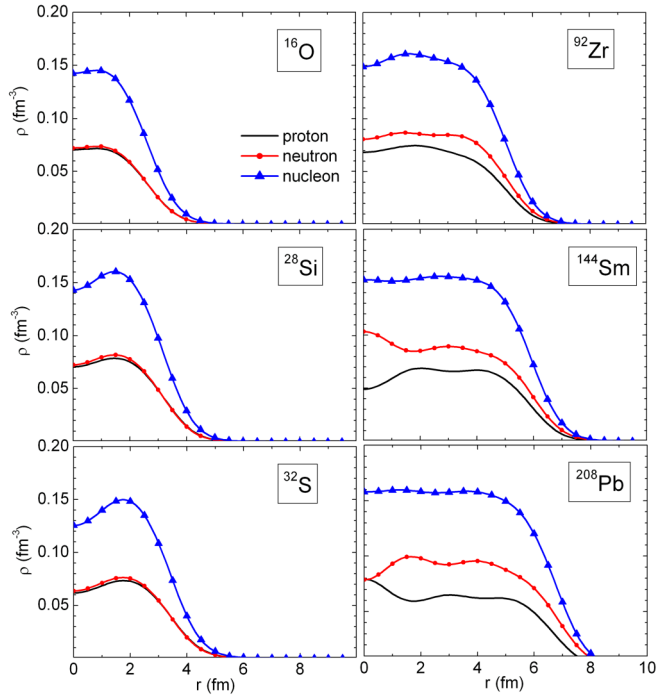

FIG. 3. (Color online) Proton, neutron, and nucleon densities obtained within the framework of the SHF approach.

C. Potential energy and nuclear matter density

Whatever is the method of calculating the capture cross section, the SnnP plays a key role. We use here the double-folding potential (DFP) with the density-dependent M3Y *NN* forces. The finite-range exchange forces are used. Description of this potential can be found in many papers (see, e.g. [9,10]) therefore we do not repeat it here. The parameters of the DFP applied in this work are exactly the same as in [18]. The least defined ingredient of the DFP is the nuclear matter density. In many works [4–6,9,10,35,36] the 2pF ansatz (2) was used for it. In the present work the nuclear matter density is calculated using the Skyrme-Hartree-Fock approach with the tensor forces as described in [37,38] with the SKP parametrization of Ref. [39].

The resulting density distributions are displayed in Fig. 3. In each panel three densities are shown: the proton (line without symbols), neutron (line with dots), and nucleon (line with triangles) densities. We see that the SHF proton densities rarely possess the 2pF shape. Yet the SHF nucleon densities for ^{16}O, ^{92}Zr, ^{144}Sm, and ^{208}Pb resemble the 2pF profiles very much. On the other hand, since the SnnP is defined by the tails of the density distributions, one probably should not pay too much attention to the difference between the SHF and 2pF densities in the interior of the nucleus.

In order to compare the calculated densities with the experimental ones we present in Fig. 4 the charge densities multiplied by factor r^2 for all six nuclei. Exactly this construction ρr^2 enters the folding integrals used for nucleus-nucleus potential calculations. As the experimental data, we use the results of the Fourier-Bessel analysis made in [11]. Figure 4 demonstrates rather good agreement of the calculated and experimental densities, especially for the heavier nuclei.

An important characteristic of the distribution is the rms charge radius on which precise and systematic data are presently available [40]. Calculated rms charge radii are compared to the data in Fig. 5. One sees that the agreement is very good for the heavy nuclei (the target nuclei of our reactions) whereas for the lighter (projectile) nuclei it becomes worse. The maximum fractional error reaches 5% for ^{16}O.

It is useful to investigate the influence of the tensor forces applied in the SHF approach for the nuclear matter density calculations on the final results of the dynamical modeling. For this aim we present in Fig. 6 the ratio of the cross sections calculated accounting for the tensor forces, σ_{tens}, over the cross sections without those, σ_0. One sees that accounting for the tensor forces enhances the cross sections by 7–15% depending upon the collision energy. This enhancement is significant for the analysis of the data possessing 1% error.

For the dynamical modeling of the nucleus-nucleus collisions, the DFP obtained by evaluation of the proper integrals is approximated using the Gross-Kalinowski profile [7]:

$$U_n(R) = -\ln\left\{1+\exp\left(-\frac{\Delta R}{a_{\text{GK}}}\right)\right\} \times [A_{0\text{GK}} + A_{1\text{GK}}\Delta R + A_{2\text{GK}}\Delta R^2], \quad (11a)$$

$$\Delta R = R - r_{\text{GK}}\left(A_P^{1/3} + A_T^{1/3}\right). \quad (11b)$$

The coefficients r_{GK}, a_{GK}, $A_{0\text{GK}}$, $A_{1\text{GK}}$, and $A_{2\text{GK}}$ are varied to fit the double-folding potential in the range $0.8q_{B0} < q < 1.2q_{B0}$. Here q_{B0} refers to the position of the s-wave Coulomb barrier. We need to use this approximation because

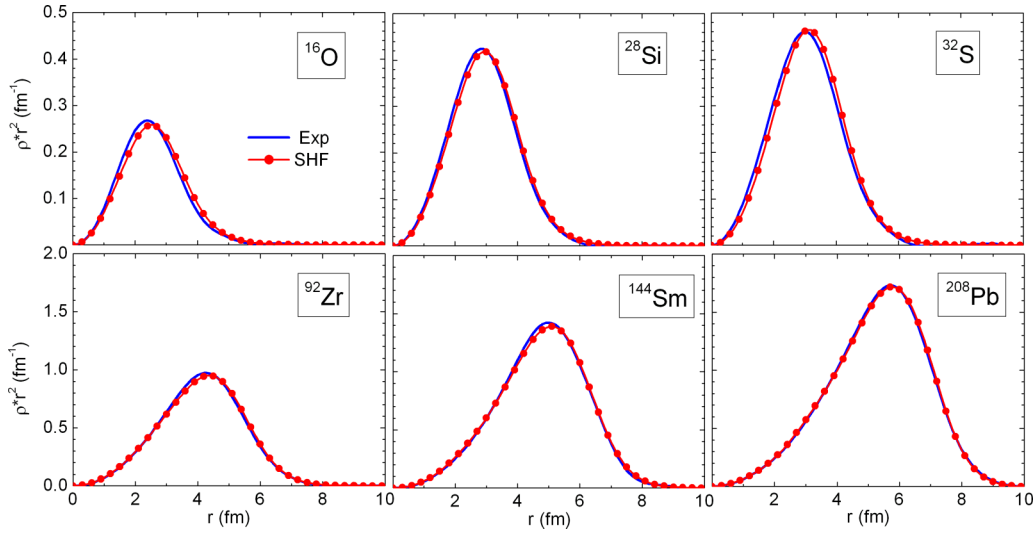

FIG. 4. (Color online) Charge density multiplied by factor r^2 calculated within the framework of the SHF approach (lines with dots) compared with the experimental one (Fourier-Bessel coefficients are taken from [11]; lines without symbols).

it is difficult to calculate the double-folding M3Y integrals accurately enough at large values of R and, consequently, q as was discussed in Refs. [4–6,18]. The parameters of the potential for these six reactions as well as for three extra reactions (see below) considered in this work are displayed in Table I.

It is interesting to compare the s-wave barrier parameters obtained in the calculations with those extracted from the analysis of the precision excitation functions [3]. This is performed in Table I. We see that the DFM potential barriers are mostly lower then the experimental ones: $^{16}\mathrm{O} + {}^{208}\mathrm{Pb}$ is the only exception. The opposite is expected in the BPM approach because the couplings to the excited states should result in even lower barriers. In the dynamical picture the effective s-wave barrier height is defined not only by the potential energy, but by the dissipation as well. These calculated dissipative barrier heights $U_{B0\mathrm{diss}}$, shown in Table I, too, are larger than the potential barrier heights. For the reactions $^{16}\mathrm{O} + {}^{208}\mathrm{Pb}$, $^{28}\mathrm{Si} + {}^{208}\mathrm{Pb}$, and $^{32}\mathrm{S} + {}^{208}\mathrm{Pb}$, $U_{B0\mathrm{diss}} > U_{B0\,\mathrm{exp}}$. This circumstance moves the whole picture closer to the reasonable and expected framework.

The last column of Table I includes the parameter a_{GK} which can be interpreted as the effective diffuseness of the potential. Indeed when ΔR in Eq. (11) becomes equal to, e.g., $3a_{\mathrm{GK}}$, the exponential function becomes a small parameter, and

$$U_n = -A_{0\mathrm{GK}} \exp\left(-\frac{\Delta R}{a_{\mathrm{GK}}}\right) \tag{12}$$

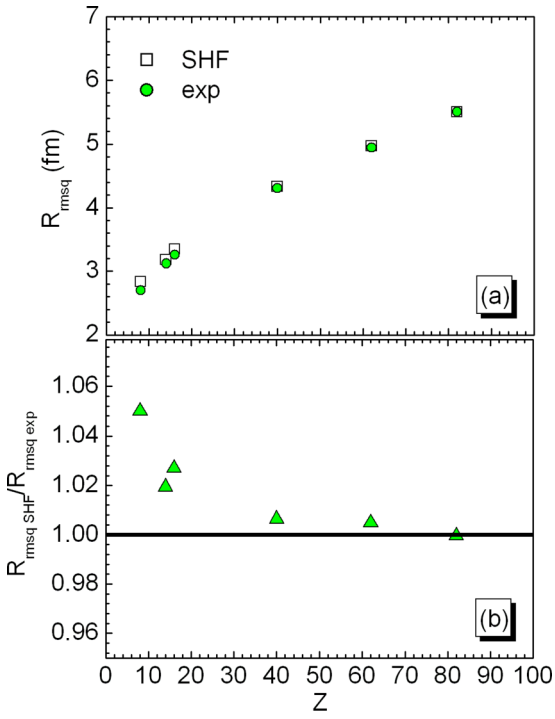

FIG. 5. (Color online) (a) Rms charge radii $R_{\mathrm{rms}q}$ obtained within the framework of the SHF approach (squares) and the experimental ones [40] (circles). (b) Ratio of the calculated rms charge radius to the experimental one.

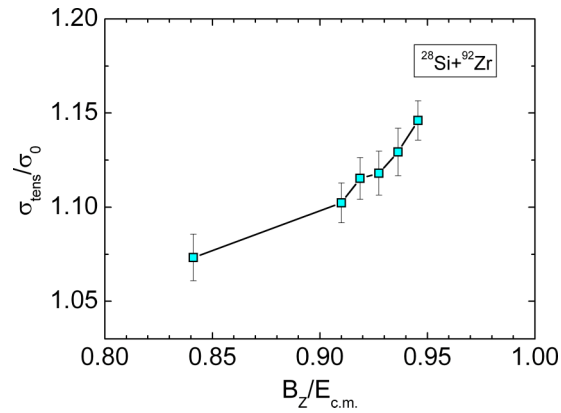

FIG. 6. (Color online) Influence of the tensor forces on the capture excitation function for the reaction $^{28}\mathrm{Si} + {}^{92}\mathrm{Zr}$.

TABLE I. Parameters of the potentials for the reactions under consideration. $U_{B0\text{expt}}$ and $R_{B0\text{expt}}$ are taken from Ref. [3] where they were extracted from the data analysis. $U_{B0\text{pot}}$ and R_{B0} are the potential barrier height and radius obtained in the present calculations. q_{B0} is the dimensionless potential barrier radius (for each reaction, it is different from that of Ref. [4] because q is defined differently). $U_{B0\text{diss}}$ is the minimum collision energy (the height of the dissipative barrier) at which the nonfluctuating dissipative trajectory overcomes the s-wave barrier (this value is obtained using $K_R = 2.0 \times 10^{-2}$ MeV^{-1} zs). The parameters of the Gross-Kalinowski profile are included, too.

Reaction	$U_{B0\text{expt}}$	$R_{B0\text{expt}}$	$U_{B0\text{pot}}$	R_{B0}	q_{B0}	$U_{B0\text{diss}}$	Coefficients of the GK approximation				
	(MeV)	(fm)	(MeV)	(fm)		(MeV)	$A_{0\text{GK}}$ (MeV)	$A_{1\text{GK}}$ (MeV fm^{-1})	$A_{2\text{GK}}$ (MeV fm^{-2})	r_{GK} (fm)	a_{GK} (fm)
^{16}O + ^{92}Zr	41.96	10.02	40.9	10.56	1.12	41.1	20.5	4.2	2.2	1.34	0.50
^{16}O + ^{144}Sm	61.03	10.85	59.8	11.24	1.10	60.2	23.0	0.2	0.0	1.32	0.58
^{16}O + ^{208}Pb	74.52	11.31	74.7	11.95	1.09	75.3	26.0	1.6	0.0	1.30	0.56
^{28}Si + ^{92}Zr	70.93	10.19	69.7	10.84	1.11	70.3	28.5	1.2	0.0	1.30	0.58
^{28}Si + ^{208}Pb	128.07	11.45	127.7	12.23	1.06	129.8	25.5	0.2	0.0	1.30	0.56
^{32}S + ^{208}Pb	144.03	10.91	143.9	12.39	1.05	146.6	28.0	1.0	0.0	1.30	0.56
^{16}O + ^{16}O	–	–	9.69	8.83	1.31	9.8	20.5	4.6	0.2	1.34	0.56
^{16}O + ^{28}Si	–	–	16.43	9.14	1.25	16.5	22.5	4.8	0.0	1.32	0.56
^{28}Si + ^{28}Si	–	–	27.88	9.44	1.18	27.9	21.5	3.6	0.0	1.32	0.56

(here we take into account that $A_{0\text{GK}}$ is much larger than two other terms of the polynomial). Equation (12) resembles very much the limiting shape of the Woods-Saxon profile (1) at $\Delta R = R - r_{\text{WS}}(A_P^{1/3} + A_T^{1/3}) >> a_{\text{WS}}$:

$$U_n = V_{\text{WS}} \exp\left(-\frac{\Delta R}{a_{\text{WS}}}\right). \tag{13}$$

Thus our double-folding potential indeed possesses normal (small) diffuseness of about 0.5-0.6 fm.

IV. COMPARING CALCULATED CROSS SECTIONS WITH THE DATA

The calculated capture excitation functions are compared with the data (semi-open circles) in Fig. 7. Results obtained with $K_R = 2.0 \times 10^{-2}$ MeV$^{-1} \cdot$ zs (which is close to 3.5×10^{-2} MeV$^{-1} \cdot$ zs reported in [8]) are shown by triangles, the BPM cross sections are presented by the thick black lines. The typical statistical error of the dynamical calculation is 1%, and the typical number of trajectories resulting to capture is 5×10^4 to 1×10^6. The BPM cross sections obtained with the SnnP possessing small diffuseness are known to exceed the data. This is observed in all the panels of Fig. 7.

The dynamical cross sections lie below the BPM ones as it is expected. In the case of ^{16}O + ^{92}Zr the dynamical calculation significantly overestimates the data; for ^{16}O + ^{144}Sm, ^{16}O + ^{208}Pb, and ^{28}Si + ^{92}Zr the dynamical excitation functions are in qualitative agreement with the data; whereas for ^{28}Si + ^{208}Pb and ^{32}S + ^{208}Pb the calculated cross sections lie below the data. This might suggest the dependence of the friction strength coefficient upon the system.

Following this indication we varied the value of K_R searching for the minimal value of χ^2 averaged over the number of points ν, χ^2_ν:

$$\chi^2_\nu = \frac{1}{\nu} \sum_{i=1}^{\nu} \left(\frac{\sigma_{i\,\text{theor}} - \sigma_{i\text{expt}}}{\Delta\sigma_{i\text{expt}}}\right)^2. \tag{14}$$

Here $\sigma_{i\,\text{theor}}$ is the theoretical value of the cross section at the particular value of $E_{\text{c.m.}\,i}$, $\sigma_{i\text{expt}}$ and $\Delta\sigma_{i\text{expt}}$ are the experimental values of the cross section and its error at the same energy. The resulting cross sections divided by the experimental ones, $\xi = \sigma_{\text{theor}}/\sigma_{\text{expt}}$, are shown in Fig. 8. The values of K_R providing the minimal χ^2_ν values are indicated in the figure. First, all the points but four lie within the 10% interval. This in our opinion indicates that the model reflects the correct physics in general. Second, more than half of

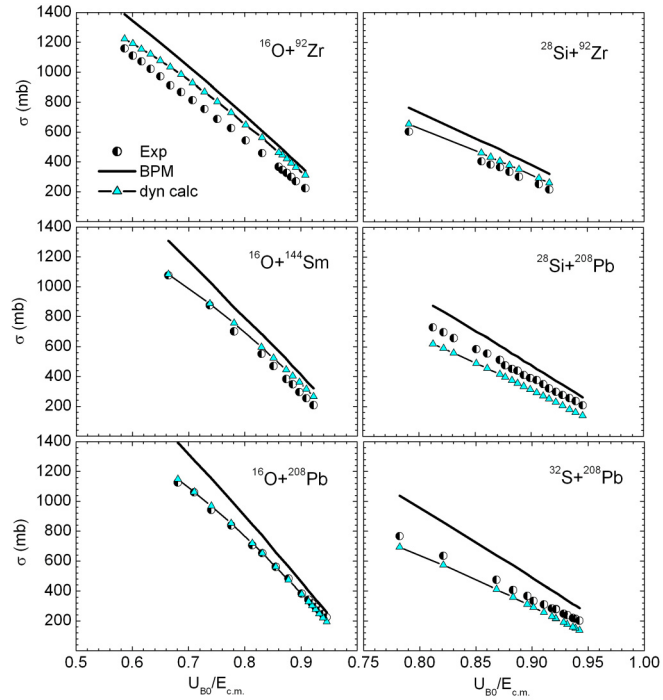

FIG. 7. (Color online) Calculated cross sections compared to the data (semi-open circles). Lines without symbols display results of the BPM calculations; lines with triangles are for the dynamical calculations. $K_R = 2.0 \times 10^{-2}$ MeV^{-1} zs.

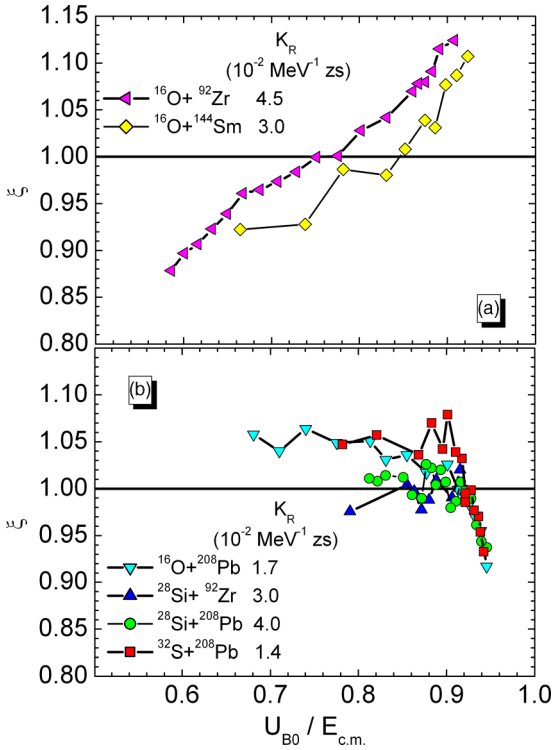

FIG. 8. (Color online) Ratio $\xi = \sigma_{\rm theor}/\sigma_{\rm expt}$ as the function of $U_{B0}/E_{\rm c.m.}$for the six reactions for which the precision data are available: (a) for two lighter systems; (b) for four heavier systems. These calculations were done with the values of K_R (shown in the figures) providing the minimum value of χ^2_ν for each reaction.

the points come out beyond the 2% interval required by the high-precision data. This means that some ingredients are still missing in our model.

In Fig. 8(a) the results for ^{16}O + ^{92}Zr and ^{16}O + ^{144}Sm reactions are shown. The corresponding curves cross the horizontal line $\xi = 1$ from left-bottom to right-top. They cannot be brought closer to unity because of the monotonic dependence upon $U_{B0}/E_{\rm c.m.}$. We checked whether the reduced

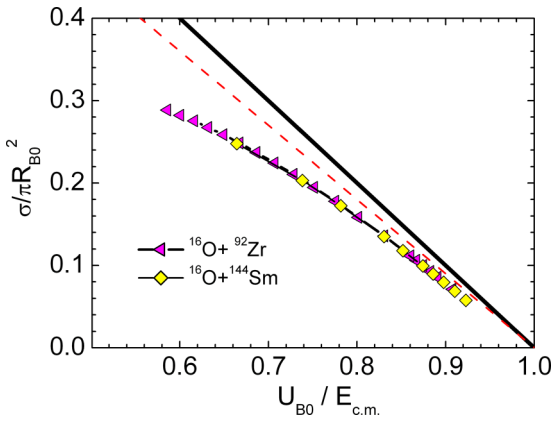

FIG. 9. (Color online) Calculated reduced cross sections for ^{16}O + ^{92}Zr and ^{16}O + ^{144}Sm. Thin dashed line corresponds to Eq. (3) times 0.9; thick solid line represents Eq. (3).

cross sections for these two reactions followed the expected linear behavior as functions of $U_{B0}/E_{\rm c.m.}$ (see Fig. 1). Results of the calculations shown in Fig. 9 clearly demonstrate that they do not.

We suggest that the reason for this failure is the incorrect density distribution for ^{16}O resulting from the present SHF calculations. This suggestion is in accord with the maximum deviation of the calculated rms charge radius from the data observed for ^{16}O in Fig. 5. In order to confirm or disprove this hypothesis we invoked the data on three more reactions: ^{16}O + ^{16}O, ^{16}O + ^{28}Si, and ^{28}Si + ^{28}Si. Calculations are compared to those data in Fig. 10. Specific features of the symmetric reactions with the nuclei in 0^+ states are accounted

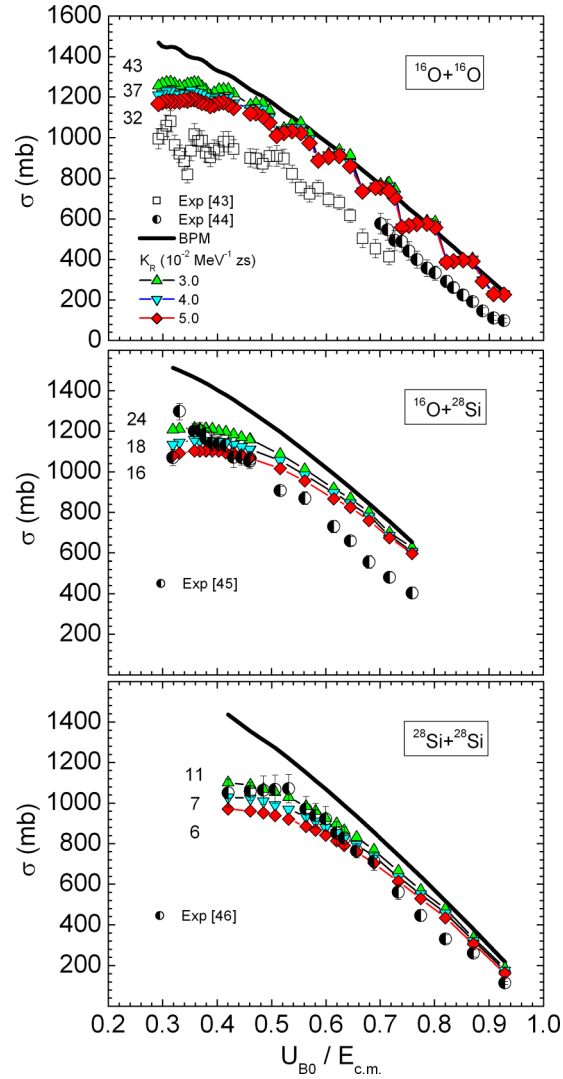

FIG. 10. (Color online) Calculated cross sections compared to the data (open and semi-open symbols). Solid thick line displays results of the BPM calculations. Triangles up, triangles down, and diamonds correspond to dynamical calculations with $K_R = 3.0$, 4.0, and 5.0 (in units of 10^{-2} MeV^{-1}zs), respectively. The data are taken from [43,44] for ^{16}O + ^{16}O, from [45] for ^{16}O + ^{28}Si, and from [46] for ^{28}Si + ^{28}Si. Digits next to lines with symbols indicate the values of χ^2_ν.

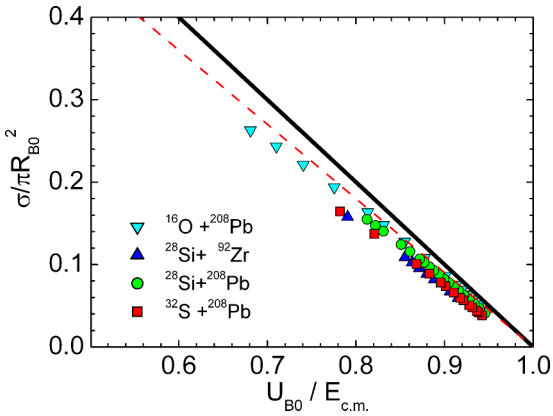

FIG. 11. (Color online) Reduced cross sections for $^{16}O + ^{208}Pb$, $^{28}Si + ^{92}Zr$, $^{28}Si + ^{208}Pb$, and $^{32}S + ^{208}Pb$. Thin dashed line corresponds to Eq. (3) times 0.9; thick solid line represents Eq. (3).

for in these calculations. Although the data possess rather large errors (about 10%) one clearly sees that the calculated excitation function cannot be brought into agreement with the data for the $^{16}O + ^{16}O$ reaction. For this reaction the cross sections are not sensitive to the value of K_R.

In order to understand the oscillations of the dynamical cross sections at low collision energies for the $^{16}O + ^{16}O$ reaction let us inspect Eq. (9). Consider first the situation without thermal fluctuations and keep in mind that L is considered as the discrete variable (which it is in reality). As the collision energy increases, the multiplier in front of the sum decreases in a continuous manner whereas $L_{\max}$ and consequently the whole sum abruptly increase. This inevitably results in the kinks in the excitation function. Thermal fluctuations smear out these kinks for heavier systems and for higher collision energies (we saw in Fig. 2 that fluctuations are more pronounced for the heavier systems). More details can be found in Refs. [4,41,42].

For the $^{16}O + ^{28}Si$ reaction the situation looks somewhat better: the minimal value $\chi^2_\nu = 16$ at $K_R = 5.0 \times 10^{-2}$ MeV^{-1} zs results from the calculation (digits next to lines with symbols indicate the values of χ^2_ν). Finally, for $^{28}Si + ^{28}Si$ reaction, minimal $\chi^2_\nu = 6$ at $K_R = 5.0 \times 10^{-2}$ MeV^{-1} zs is achieved. Note that in Ref. [41] the experimental fusion excitation function in reaction $^{16}O + ^{16}O$ is well described by the TDHF calculations.

Let us now come back to the reactions on which the high-precision data are available. For the remaining four reactions the reduced cross sections versus $U_{B0}/E_{\text{c.m.}}$ are presented in Fig. 11. They are significantly closer to the expected linear trend. Inspecting the curves $\xi\,(U_{B0}/E_{\text{c.m.}})$ for these reactions in Fig. 8(b) more attentively one sees that the corresponding ratios are approximately parallel to unity for $U_{B0}/E_{\text{c.m.}} < 0.9$ and decrease for smaller collision energies (right parts of the curves). Let us recall that our model does not account for the couplings to the vibrational states, which is expected to play an increasingly important role for lower collision energies. Selecting the data for our analysis we followed Ref. [3] where rather arbitrary border $\sigma > 200$ mb was taken. Comparison of our results with the data presented in Fig. 8(b) suggests that a criterion $U_{B0}/E_{\text{c.m.}} < 0.9$ probably is to be used instead of $\sigma > 200$ mb.

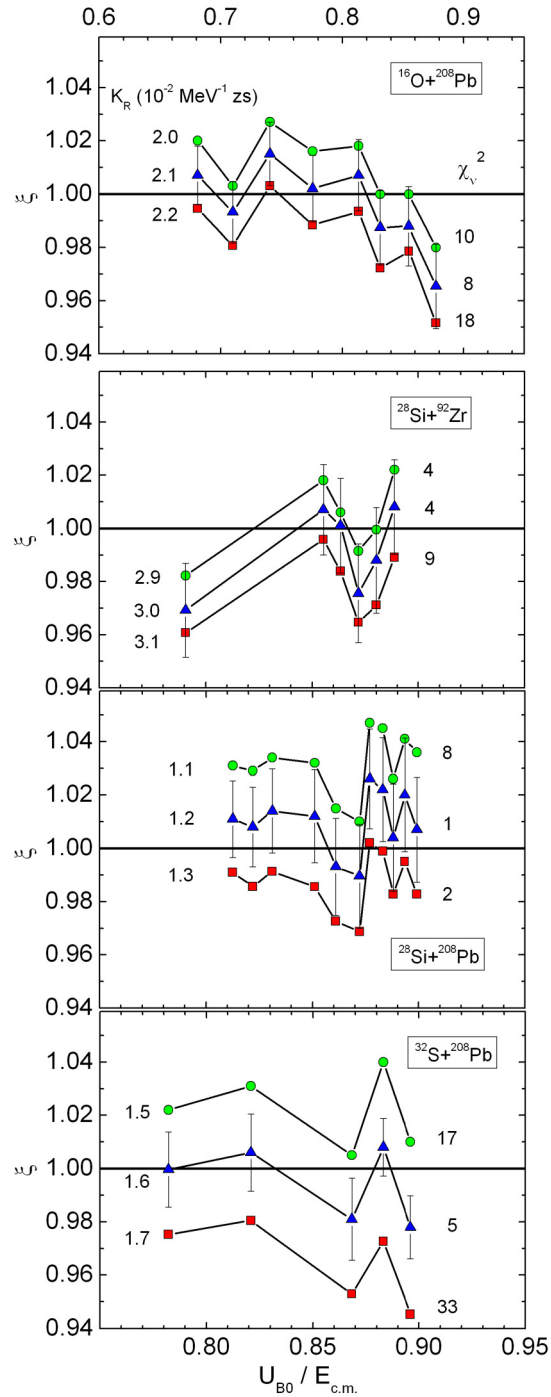

FIG. 12. (Color online) The ratio $\xi = \sigma_{\text{theor}}/\sigma_{\text{expt}}$ of the calculated cross section to the experimental one for $U_{B0}/E_{\text{c.m.}} < 0.90$. Digits left of lines indicate the values of the dissipation strength coefficient $K_R/(10^{-2}$ MeV^{-1} zs). Digits right of lines indicate the values of χ^2_ν. The error bars represent the experimental errors. The number of trajectories is large enough to make the statistical errors of the calculations negligible.

One can argue that if the density distribution for ^{16}O resulting from the present SHF calculations is incorrect, the

agreement of our calculations with the data should be poor for the reaction $^{16}O + ^{208}Pb$ also. We cannot disprove this objection. However, the reaction $^{16}O + ^{208}Pb$ is known to be a hard nut as discussed in the Introduction of Ref. [3] and in Ref. [15]. This reaction is one of few (if not the only one) for which in Ref. [15] no reasonable fit of the above- and below-barrier data was reached with the same diffuseness of the potential.

We varied again the value of K_R, searching for the minimum of χ^2_ν for the sets of the data for $^{16}O + ^{208}Pb$, $^{28}Si + ^{92}Zr$, $^{28}Si + ^{208}Pb$, and $^{32}S + ^{208}Pb$ cut at $U_{B0}/E_{c.m.} = 0.9$. Results of these calculations are displayed in Fig. 12 along with the values of K_R and χ^2_ν. It turns out that the values of χ^2_ν from 8 down to 1 can be achieved with rather reasonable values of K_R ranging from 3.0×10^{-2} to 1.2×10^{-2} MeV^{-1} zs.

Comparing the panels corresponding to different reactions we can conclude that the calculated cross sections become more sensitive to the value of K_R as $Z_P Z_T$ increases. Moreover, the value of K_R providing the minimal value of χ^2_ν seems to decrease as $Z_P Z_T$ increases (although the value of K_R for the reaction $^{32}S + ^{208}Pb$ is somewhat larger than for the lighter reaction $^{28}Si + ^{208}Pb$). The value $K_R = (4 - 5) \times 10^{-2}$ MeV^{-1} zs at which the minimal $\chi^2_\nu = 7$ to 6 is reached for $^{28}Si + ^{28}Si$ reaction [Fig. 10(c)] corroborates this conclusion. This decrease correlates with the decrease of the q_{B0} value.

Presently, we do not have a physical explanation for the decrease of the K_R value with $Z_P Z_T$. Trying to think about such an explanation, one has to keep in mind that the friction coefficient in the dissipative force is defined not only by its strength K_R but also by the form factor $(dU_n/dq)^2$ which becomes larger due to the smaller q_{B0} value as $Z_P Z_T$ increases. We prefer not to go deeper into this question before more systematic calculations (for the reactions involving deformed target nuclei) are made and the effect of the K_R decrease is firmly established (if it is done).

V. CONCLUSIONS

We calculate the capture (fusion) cross sections for nine reactions involving spherical nuclei: $^{16}O + ^{16}O$, ^{28}Si, ^{92}Zr, ^{144}Sm, ^{208}Pb; $^{28}Si + ^{28}Si$, ^{92}Zr, ^{208}Pb; $^{32}S + ^{208}Pb$. For six of these reactions the experimental errors are about 1%, whereas for the $^{16}O + ^{16}O$, $^{16}O + ^{28}Si$, and $^{28}Si + ^{28}Si$ reactions the errors are about 10%. When the high-energy parts ($\sigma > 200$ mb) of the six high-precision experimental excitation functions were analyzed earlier within the framework of the single-barrier penetration model based on the Woods-Saxon profile for the SnnP, the problem of the apparently large diffuseness of the SnnP appeared [3]. We applied our fluctuation-dissipation trajectory model to the quantitative analysis of these high-precision data varying the radial friction strength coefficient. The core of the model is the double-folding approach with the density-dependent M3Y *NN* forces including the finite-range exchange part. The nuclear matter densities required to evaluate the folding integrals are obtained using the Skyrme-Hartree-Fock approach including the tensor interaction [37,38,39]. The resulting nucleus-nucleus potentials have rather small (normal) diffusenesses. Our calculations demonstrated that

(1) The high-precision data on six reactions can be reproduced within 10% in the framework of our model at the collision energies 10% above the calculated potential barrier.
(2) For the reactions induced by ^{16}O (except $^{16}O + ^{208}Pb$) the calculated cross sections cannot be brought into agreement with the data within the experimental errors. This suggests that the nuclear density calculated for ^{16}O is incorrect. This statement is confirmed by the comparison between calculated and experimental rms charge radii and by the analysis of the less precise capture data on $^{16}O + ^{16}O$ and $^{16}O + ^{28}Si$ reactions.
(3) For reactions not involving ^{16}O and, surprisingly, for the $^{16}O + ^{208}Pb$ reaction the agreement with the data within 3% is achieved with K_R ranging from 3.0×10^{-2} to 1.2×10^{-2} MeV^{-1} zs which does not contradict the previous works [4,7,8].
(4) The calculated capture cross sections become more sensitive to the value of K_R as $Z_P Z_T$ increases.
(5) A trend of K_R to decrease as $Z_P Z_T$ increases is revealed.

ACKNOWLEDGMENT

M.V.C. is grateful to the Dmitry Zimin "Dynasty" Foundation for their financial support.

[1] M. Dasgupta, D. J. Hinde, N. Rowley, and A. M. Stefanini, Annu. Rev. Nucl. Part. Sci. **48**, 401 (1998).
[2] K. Hagino, N. Rowley, and A. T. Kruppa, Comput. Phys. Commun. **123**, 143 (1999).
[3] J. O. Newton, R. D. Butt, M. Dasgupta, D. J. Hinde, I. I. Gontchar, C. R. Morton, and K. Hagino, Phys. Rev. C **70**, 024605 (2004).
[4] M. V. Chushnyakova and I. I. Gontchar, Phys. Rev. C **87**, 014614 (2013).
[5] M.V. Chushnyakova and I. I. Gontchar, EPJ Web Conf. **63**, 02008 (2013).
[6] M. V. Chushnyakova and I. I. Gontchar, EJP Web Conf. (to be published).
[7] D. H. E. Gross and H. Kalinowski, Phys. Rep. **45**, 175 (1978).
[8] P. Fröbrich, Phys. Rep. **116**, 337 (1984).
[9] Dao T. Khoa, G. R. Satchler, and W. von Oertzen, Phys. Rev. C **56**, 954 (1997).
[10] I. I. Gontchar and M. V. Chushnyakova, Comput. Phys. Commun. **181**, 168 (2010).
[11] H. de Vries, C. W. de Jager, and C. de Vries, At. Data Nucl. Data Tables **36**, 495 (1987).
[12] http://nrv.jinr.ru/nrv/webnrv/fusion/reactions.php
[13] J. O. Newton, C. R. Morton, M. Dasgupta, J. R. Leigh, J. C. Mein, D. J. Hinde, H. Timmers, and K. Hagino, Phys. Rev. C **64**, 064608 (2001).

[14] J. R. Leigh, M. Dasgupta, D. J. Hinde, J. C. Mein, C. R. Morton, R. C. Lemmon, J. P. Lestone, J. O. Newton, H. Timmers, J. X. Wei, and N. Rowley, Phys. Rev. C **52**, 3151 (1995).
[15] C. R. Morton, A. C. Berriman, M. Dasgupta, D. J. Hinde, J. O. Newton, K. Hagino, and I. J. Thompson, Phys. Rev. C **60**, 044608 (1999).
[16] D. J. Hinde, C. R. Morton, M. Dasgupta, J. R. Leigh, J. C. Mein, and H. Timmers, Nucl. Phys. A **592**, 271 (1995).
[17] C. Y. Wong, Phys. Rev. Lett. **31**, 766 (1973).
[18] M. V. Chushnyakova and I. I. Gontchar, J. Phys. G **40**, 095108 (2013).
[19] C. Simenel, Phys. Rev. Lett. **105**, 192701 (2010).
[20] Lu Guo and Takashi Nakatsukasa, EPJ Web Conf. **38**, 09003 (2012).
[21] A. S. Umar and V. E. Oberacker, Phys. Rev. C **73**, 054607 (2006).
[22] C. Simenel, Eur. Phys. J. A **48**, 152 (2012).
[23] R. Keser, A. S. Umar, and V. E. Oberacker, Phys. Rev. C **85**, 044606 (2012).
[24] R. T. deSouza, S. Hudan, V. E. Oberacker, and A. S. Umar, Phys. Rev. C **88**, 014602 (2013).
[25] K. Wen, F. Sakata, Z.-X. Li, X.-Z. Wu, Y.-X. Zhang, and S.-G. Zhou, Phys. Rev. Lett. **111**, 012501 (2013).
[26] I. I. Gontchar, D. J. Hinde, M. Dasgupta, and J. O. Newton, Phys. Rev. C **69**, 024610 (2004).
[27] J. Marten and P. Fröbrich, Nucl. Phys. A **545**, 854 (1992).
[28] P. Fröbrich and I. I. Gontchar, Phys. Rep. **292**, 131 (1998).
[29] R. A. Kuzyakin, V. V. Sargsyan, G. G. Adamian, N. V. Antonenko, E. E. Saperstein, and S. V. Tolokonnikov, Phys. Rev. C **85**, 034612 (2012).
[30] V. Zagrebaev and W. Greiner, J. Phys. G **31**, 825 (2005).
[31] V. L. Litnevsky, G. I. Kosenko, F. A. Ivanyuk, and V. V. Pashkevich, Phys. At. Nucl. **75**, 1500 (2012).
[32] A. V. Ignatyuk, M. G. Itkis, V. N. Okolovich, G. N. Smirenkin, and A. S. Tishin, Sov. J. Nucl. Phys. **21**, 612 (1975).
[33] P. Fröbrich and R. Lipperheide, *Theory of Nuclear Reactions*, Oxford Studies in Nuclear Physics Vol. 18 (Oxford University, Oxford, 1996).
[34] D. L. Hill and J. A. Wheeler, Phys. Rev. **89**, 1102 (1953).
[35] G. R. Satchler and W. G. Love, Phys. Rep. **55**, 183 (1979).
[36] V. I. Zagrebaev, A. V. Karpov, Y. Aritomo, M. A. Naumenko, and W. Greiner, Phys. Part. Nucl. **38**, 469 (2007).
[37] R. Bhattacharya, Nucl. Phys. A **913**, 1 (2013).
[38] R. Bhattacharya, J. Mod. Phys. **4**, 33 (2013).
[39] J. Dobaczewski, H. Flocard, and J. Treiner, Nucl. Phys. A **422**, 103 (1984).
[40] I. Angeli, At. Dat. Nucl. Dat. Tables **87**, 185 (2004).
[41] C. Simenel, R. Keser, A. S. Umar, and V. E. Oberacker, Phys. Rev. C **88**, 024617 (2013).
[42] H. Esbensen, Phys. Rev. C **77**, 054608 (2008).
[43] I. Tserruya, Y. Eisen, D. Pelte, A. Gavron, H. Oeschler, D. Berndt, and H. L. Harney, Phys. Rev. C **18**, 1688 (1978).
[44] A. Kuronen, J. Keinonen, and P. Tikkanen, Phys. Rev. C **35**, 591 (1987).
[45] R. Rascher, W. F. J. Muller, and K. P. Lieb, Phys. Rev. C **20**, 1028 (1979).
[46] Y. Nagashima, J. Schimizu, T. Nakagawa, Y. Fukuchi, W. Yokota, K. Furuno, M. Yamanouchi, S. M. Lee, N. X. Dai, T. Mikumo, and T. Motobayashi, Phys. Rev. C **33**, 176 (1986).